Larix Publications

Singapore Journal of Cardiology
https://sjcjournal.com/

Vol. 1, Issue 3, 2020 ISSN: 2737-4025

Original Article

Prerequisite for projection data and reconstruction not to cause truncation artifacts in myocardial perfusion single- photon emission computed tomography: Phantom study

Kotatsu Tsuboi[1, 2], Masahisa Onoguchi*[2], Mitsuo Sugimoto[3], Takayuki Shibutani[2], Akio Nagaki[4] and Akihiro Kikuchi[5]

[1] Department of Radiological Technology, Hamamatsu Red Cross Hospital, Japan
[2] Department of Quantum Medical Technology, Graduate School of Medical Sciences, Kanazawa University, Japan
[3] Department of Radiology, Nagoya Daini Red Cross Hospital, Japan
[4] Department of Radiological Technology, Kurashiki Central Hospital, Japan
[5] Department of Radiological Technology, Faculty of Health Sciences, Hokkaido University of Science, Japan

**onoguchi@staff.kanazawa-u.ac.jp*

Received on: 31-08-2020; Revised and Accepted on: 09-09-2020

ABSTRACT

Myocardial perfusion single-photon emission computed tomography (SPECT) studies are used widely in the evaluation and diagnosis of coronary artery disease. Although one method to improve the spatial resolution is zooming acquisition, truncation artifact occurs in reconstructed tomographic images. To date, it is unclear how much truncation (area and radioactivity) of projection data would affect myocardial image.

The aim of this study is to investigate the combination of truncated projection data conditions and image reconstruction methods that do not require re-examination. We used a cylindrical and anthropomorphic torso phantom with 99mTc solution, and shifted the projection data to simulate truncated liver tissue. SPECT images were acquired using a dual-detector gamma camera and reconstructed using filtered back projection (FBP) and ordered subset expectation maximization (OSEM) to create transverse images. We compared truncation data and reference data (none truncated projection data) for count profile curve, uniformity, myocardial counts, and % uptake.

Our findings indicate that prerequisite for truncation data and image reconstruction method would not affect the myocardial image, when the area of truncation was < 17.5% and the count of the truncation portion was lower than that in the myocardium using FBP.

Keywords: *Myocardium, single-photon emission computed tomography, filtered back projection.*

1. INTRODUCTION:

Myocardial perfusion single-photon emission computed tomography (SPECT) studies are used widely in the evaluation and diagnosis of coronary artery disease [1]. However, the spatial resolution for SPECT imaging is lower than that of other modalities. One method to improve the spatial resolution is zooming acquisition [2]. The acquisition may cause the loss of right-side body radioactivity outside the field of view (FOV), if heart is placed in the center of acquisition orbit. According to the principle of tomography, images cannot be reconstructed accurately using truncated projection data [3]. Therefore, an artifact, known as a truncation artifact occurs in reconstructed tomographic images [4- 10].

Most studies of truncation artifacts in myocardial perfusion SPECT have reported on the effects of the attenuation maps generated from a truncated transmission data on the reconstructed image [4-7]. On the other hand, a few studies have investigated whether the truncation artifact affects the myocardial image without attenuation correction if the myocardial image is not truncated outside the FOV at any

***Corresponding author**:

Masahisa Onoguchi,
Department of Quantum Medical Technology, Graduate School of Medical Sciences, Kanazawa University Kodatsuno 5-11-80, Kanazawa, Ishikawa 920-0942, Japan.
Email: onoguchi@staff.kanazawa-u.ac.jp
Phone: +81 76 265 2526
DOI: doi.org/10.46978/sjc.20.1.2.14

projection view, but the radioactivity of body tissue is truncated at some views [8-10]. Image reconstructed from truncated projection data display various artifacts and distortions. A ring- shaped high-count artifact that appears on the truncation edge is one of the truncation artifacts [5,7,8,10]. Apart from the artifacts, truncated projection data affect counts and uniformity in reconstructed myocardial image if truncated area becomes large [8-10]. Also, severity of truncation artifact by the difference of image reconstruction method have been discussed in previous studies [9-10].

Few studies have attempted to investigate the influence of radioactivity concentration in truncation portion such as lung or liver on the myocardial image. In addition, it has not been found that how much area of truncation affects the myocardial image. Moreover, Rohmer et al. found that small inaccuracies in image reconstructed from truncated projection data have little effect on clinical interpretation [8]. For these reasons, even if the projection data was truncated in clinical examination, we could not determine the need for re-examination.

We hypothesized that the effect of truncation artifacts for the myocardial image depends on the area and radioactivity concentration in the truncation portion and the difference of image reconstruction method. The aim of this study is to investigate the necessary prerequisite for projection data conditions and image reconstruction method that do not require re-examination.

2. METHODS

2.1 Phantoms

A cylindrical phantom (JSP type, Kyoto Kagaku Co., Ltd., Kyoto, Japan) was used. The cylindrical phantom had a diameter and height of 22.0 cm. The phantom was filled with 90.0 kBq/mL of 99mTc solution. Moreover, an anthropomorphic torso phantom (HL type, Kyoto Kagaku Co., Ltd., Kyoto, Japan) containing shapes of the normal myocardium, lungs, spine, and liver was also used. The phantom was representative of the torso of a medium-sized adult. The myocardium was filled with 90.0 kBq/mL of 99mTc solution. The liver was filled with varying concentrations of 99mTc solution so that the heart–liver relative radioactivity concentration ratios (HL radioactivity ratios) were 1:0.25, 1:0.5, and 1:1.0. We also prepared a water-filled liver so that the HL radioactivity ratio was 1:0. The left ventricular cavity, right ventricle, and mediastinum were filled with water. The lungs contained beads of polystyrene foam without radioactivity. The liver was the truncated region.

2.2 Acquisition and image processing

SPECT images were acquired using a dual-detector gamma camera (BrightView, Philips Healthcare, Cleveland, OH, USA) equipped with a low-energy high-resolution collimator. A total of 64 projection images were obtained from a 180° elliptical orbit (90° per detector) with a 40.9-cm detector mask (zoom, 1.46) and matrix size of 64×64. The projection data were acquired for 30 s per projection. A 20% energy window was set symmetrically over 140 keV of 99mTc. Projection data were processed using the JETStream Workspace (Philips Healthcare), and images were reconstructed using filtered back projection (FBP) and ordered subset expectation maximization (OSEM) to create transverse images. In FBP, a preprocessing Butterworth filter with a cutoff frequency of 0.39 cycles/cm, an order of 8, and a ramp filter were used. In OSEM, a preprocessing Butterworth filter with a cutoff frequency of 0.39 cycles/cm and an order of 8 were used with 3 iterations and 16 subsets. The parameters are the same as the clinical default reconstruction in our institution. No attenuation or scatter correction was used. The cylindrical phantom was placed in the center of the FOV and used as a reference image. The center of rotation in SPECT was shifted from the center of the phantom while being visually monitored with an emission monitor at the anterior view of projection data, and images were obtained to truncate the right side (toward the liver) of the phantom. A reference image and truncation images with 4 different areas of truncation were acquired (c1–c4). In the anthropomorphic torso phantom, a reference image and truncation images with 3 different areas of truncation were acquired (a1–a3). SPECT images were acquired 6 times at each position. Count profile curves were determined in the horizontal direction of the center of the transverse image for the cylindrical phantom. In the anthropomorphic torso phantom, the count profile curves were determined in the horizontal direction at the level of the heart. The area of truncation was calculated

Using the following equation:

Area of truncation = (A-B) / A×100%,

where A is the phantom diameter of the reference image in the FOV and B is the phantom diameter in the truncation image in the FOV (Fig. 1). The A and B of the diameters were calculated from the count profile curve. The transverse images of the cylindrical and anthropomorphic torso phantoms are shown in Fig. 2. In the cylindrical phantom, the areas of truncation for c1, c2, c3, and c4 were 18.2 ± 0, 29.7 ± 0, 37.8 ± 0, and 51.4 ± 0%, respectively. In the anthropomorphic torso phantom, the areas of truncation for a1, a2, and a3 were 17.5 ± 2.1, 32.9 ± 1.4, and 49.1 ± 1.4%, respectively. The projection data for the anterior view are presented in Fig. 3. The liver-to-myocardium count ratios per pixel were 1.21 ± 0.02, 2.32 ± 0.22, and 4.03 ± 0.10 for HL radioactivity ratios 1:0.25, 1:0.5, and 1:1.0, respectively. We used the Daemon Research Image Processor (FUJIFILM Toyama Chemical Co., Ltd, Tokyo, Japan) in the image analysis and quantitative perfusion SPECT (Cedars-Sinai Medical Center, Los Angeles, CA, USA), version 7.0, in the polar map creation.

2.3. Image evaluation

The mean count profile curves were determined in the horizontal direction of the center from the average of five transverse images of the cylindrical phantom. The count profiles curves for the truncation image were visually compared with those of the reference image. Additionally, we investigated the uniformity in the FOV of the truncation data. The rectangular region of interest (ROI) was manually set on the cylindrical phantom in the FOV (Fig. 4). The coefficients of variation (CVs) of the truncation image were compared with those of the reference image. The CV was calculated as follows:

CV (%) = SD / mean × 100,

where SD and mean are the standard deviation and average value in the ROIs, respectively.

In the anthropomorphic torso phantom, we compared the myocardial counts of the truncation image with those of the reference image in the ROI on the myocardium of three consecutive slices of the transverse image. Moreover, the % uptake was calculated using the standard 17-segment model of the left ventricle [11]. In segments 7-17, the average % uptakes of the truncation image were compared to those of the reference image.

2.4. Statistical analysis

Continuous valuables were expressed as the mean ± SD. The CVs at each degree of truncation versus the reference image using the cylindrical phantom were compared using one-way repeated-measures analysis of variance. The Friedman test was used to compare the myocardial counts between the truncation and reference images. For the % uptake comparison of the polar map, the coin method was used after the Friedman test. The exact P-value in a small paired sample in many ties in the 6 observations was calculated using the R package "coin," a class of permutation test. A post hoc analysis with Bonferroni correction was performed.

A P-value of <0.05 was considered to be statistically significant. All statistical analyses were performed using EZR (Saitama Medical Center, Jichi Medical University, Saitama, Japan), a graphical user interface for R 3.3.1 (R Foundation for Statistical Computing, Vienna, Austria) [12].

3. RESULTS

3.1. Count profile curve

In the evaluation of the cylindrical phantom, both FBP and OSEM produced a high-count artifact in the truncation portion of the phantom in transverse images (Fig. 5). Compared with FBP, the artifact of OSEM was higher with a larger area of truncation. Moreover, in OSEM, a larger fluctuation in the count profile curve was observed near the high-count artifact than that in FBP.

3.2. Uniformity (CVs)

Results of the CVs are shown in Fig. 6. In FBP, the differences in the CVs were not observed between the reference and truncation data. However, in OSEM, an increase in the CVs was observed in c2, c3, and c4 of the truncation data compared to those of the reference data. The CVs were higher with the increasing area of truncation (The CVs of the reference, c2, c3, and c4 were 6.4 ± 1.0, 7.8 ± 1.2, 9.0 ± 1.4, and 14.3 ± 2.3, respectively.)

3.3. Myocardial counts

Figure 7 shows the results of the myocardial count. In the HL radioactivity ratio 1:0 of FBP, the differences in the myocardial count were not observed between the truncation and reference data.

However, in the HL radioactivity ratios 1:0.25 and 1:0.5 of FBP, an increase in the myocardial count was observed in a2 and a3 data compared to those in the reference data. In the HL radioactivity ratio 1:1.0, an increase in the myocardial count was observed in a1, a2, and a3 data compared to those in the reference data. The myocardial counts for the reference, a1, a2, and a3 were 132.3 ± 2.2, 135.5.4 ± 1.6, 147.4 ± 1.7, and 173.0 ± 1.5, respectively. Compared with the reference data, the myocardial count increase rates of a3 in FBP were 1.09, 1.15, and 1.31 for the HL radioactivity ratios of 1:0.25, 1:0.5, and 1:1.0, respectively. In OSEM, the differences in the myocardial count were not observed between the reference and truncation data in the HL radioactivity ratios 1:0 and 1:1.0. In the HL radioactivity ratio 1:0.25 in OSEM, an increase in the myocardial count was observed in a1, a2, and a3 data compared to those in the reference data. The myocardial counts for the reference, a1, 2, and a3 were 285.1 ± 5.8, 312.1 ± 4.1, 313.3 ± 4.4, and 309.5 ± 6.6, respectively. In the HL radioactivity ratio 1:0.5, an increase in the myocardial count was observed only in a3 data compared to that in the reference data. 3.4% uptake Figure 8 presents the % uptake of the polar map for the reference and truncation data. In the HL radioactivity ratio 1:0 and a1 of both FBP and OSEM, the difference in % uptake for the truncation data was not observed in all segments compared with those for the reference data. In the HL radioactivity ratio 1:0.25 of FBP, the difference in % uptake was observed in a3 data compared to that in the reference data. In the HL radioactivity ratios 1:0.5 and 1:1.0 of FBP, the difference in % uptake was observed in a2 and a3 data compared to those in the reference data.

All % uptakes of the different segments in the truncation data were higher than those in the reference data in FBP. In the HL radioactivity ratios 1:0.25, 1:0.5, and 1:1.0 of OSEM, the difference in % uptake was observed in a2 and a3 data compared to those in the reference data. The % uptake of different segments increased in a2 of the HL radioactivity ratios 1:0.25 and 1:0.5. In a2 of the HL radioactivity ratio 1:1.0 and a3 of the HL radioactivity ratios 1:0.25, 1:0.5, and 1:1.0, the % uptake increased and decreased, respectively.

In a3 of the HL radioactivity ratio 1:1.0, the % uptake decreased in segments 7, 8, 13, 14, 15, and 17 and increased in segments 9, 10, 11, and 12 compared to those in the reference data.

4. DISCUSSION

In this study, the effect of truncated projection data on myocardial image in myocardial perfusion SPECT was investigated using cylindrical and anthropomorphic torso phantoms for FBP and OSEM.

We shifted the projection data to simulate truncated liver tissue and investigated the uniformity and count of the myocardial image in the FOV. Our results supported the hypothesis that the effect of truncation artifacts depends on the area and radioactivity concentration in the truncation portion, and the difference in the image reconstruction method.

In both FBP and OSEM, the truncation data introduced a high-count artifact at the truncation edge in the cylindrical phantom. However, the count profile curve on the truncation data in OSEM was observed a larger high-count artifact and a larger fluctuation compared with those in the FBP. As a result, an increase in CVs was observed in the truncation data of the OSEM compared to those in the reference data with a larger area of truncation. An increase of CVs means decrease in uniformity within FOV. A previous study indicated that truncated transmission CT data generated artifacts and distortion in image reconstructed by the maximum likelihood expectation maximization (MLEM) compared to that in the FBP, especially for higher degrees of truncation [5]. The study also noted that the cold ring artifact near the truncation edge occurred in MLEM. Taking our results of the CVs into account, in the truncation data, OSEM may receive a greater influence on reconstructed images than FBP. Therefore, we consider that the image reconstructed by OSEM has lower uniformity within FOV than FBP.

In the anthropomorphic torso phantom, the area and radioactivity concentration in the truncated liver tissue was changed. Then, the myocardial count on the transverse image and the % uptake of the polar map were compared between the reference and truncation data. We initially had to confirm that there was no difference in the myocardial count and polar map at each heart position within the FOV between the reference and truncation data of non-radioactivity in the truncation portion (HL radioactivity ratio 1:0) [13, 14]. As a result, both FBP and OSEM showed no difference in the myocardial count and polar map in any truncation area compared to those in the reference data (HL radioactivity ratio 1:0 in Figs. 7 and 8). Rohmer et al. used a mathematical cardiac torso phantom to simulate a small cardiac SPECT camera that would be the liver outside the FOV [8]. The simulation was conducted under the condition of only a HL radioactivity ratio 1:1.0. They reported that myocardial counts increased in FBP when the liver was outside the FOV. Our data were similar to those reported by them, namely the myocardial counts in the truncation data increased in FBP compared to those in the reference data. Then, the counts increased with a larger area and a higher radioactivity concentration of the truncation portion. A SPECT image is created from the projection data. The truncated projection data include counts outside the FOV. It is assumed that the count outside the FOV caused an increase in the myocardial count of the reconstructed image. Owing to this, with an increasing count in the truncation portion, the count in the FOV is higher than the true value.

Therefore, we believe that the increase in the myocardial count of the truncation data depends on the area and the radioactivity concentration of the truncation portion in FBP. In contrast, in OSEM, although an increase in the myocardial count of a1, a2, and a3 of the HL radioactivity ratio 1:0.25 was observed, no increase in the myocardial count was observed in the truncation data of the HL radioactivity ratio 1:1.0. The increase in the myocardial count did not show a certain trend in the area and radioactivity of the truncation portion. These results may be related to the poor uniformity of OSEM observed in the cylindrical phantom.

In the polar map of FBP, an increased % uptake was observed in a3 for the HL radioactivity ratio 1:0.25 and in a2 and a3 for HL radioactivity ratios 1:0.5 and 1:1.0 compared with those in the reference data. The number of segments tended to increase from the septal side with a larger area and a higher radioactivity concentration of the truncation portion. The anthropomorphic torso phantom used in this study was tilted so that the heart and liver were in the same slice on the transverse image. Thus, the transverse image of the myocardium became a similar image to the short- axis image (Fig. 3). The truncated liver tissue was the septal side of the myocardium. Accordingly, we speculate that the segment of % uptake, which was different from that of the reference data, occurred on the septal side. In the polar map of OSEM, similar to that of FBP, different % uptakes were observed in a2 and a3 for the HL radioactivity ratios 1:0.25, 1:0.5, and 1:1.0 compared with those in the reference data. However, the % uptake of the segment not only increased but also decreased compared to those in the reference data. Laiush et al. reported that the % bias was negative on the septal, the inferior and lateral sides in OSEM in the truncation data of the liver compared with those in the data without truncation [9]. We speculate that these phenomena are characteristic of OSEM for truncation data. In the cylindrical phantom, the radioactivity concentrations inside and outside the FOV of the truncation data were similar. On the other hand, the anthropomorphic torso phantom had a larger liver as the truncation portion. Even if the radioactivity concentration in the liver was lower than that in the heart, the count per pixel of the truncated liver was higher than that in the heart (For example, the liver-to-myocardium count ratio per pixel was 2.32 ± 0.22 for the HL radioactivity ratio 1:0.5, Fig.3). In OSEM, we assume that the

decrease in uniformity observed in the cylindrical phantom may have been further enhanced in the anthropomorphic torso phantom.

For all of these reasons, in FBP, if the area of the truncation is < 17.5% (a1 of the anthropomorphic torso phantom) and the count of the liver is lower than that in the myocardium on the anterior view of the projection data, we think that the truncated projection data do not affect the myocardial image. However, in OSEM, even if the radioactivity concentration in the truncated liver tissue is lower than that in FBP, the myocardial count may be affected (HL activity ratio 1:0.25 of OSEM in Fig.7). When performing quantitative assessments, such as coronary blood flow reserve measurements using OSEM [15, 16], it should be used for data without truncation. Even if the radioactivity concentration in the truncation portion is high, when the area of truncation is ≤ 17.5%, a change in the polar map is not recognized in both FBP and OSEM compared with those in the data without truncation. In contrast, when the area of truncation is > 17.5%, the polar map differs from those in the reference data with a larger area and a higher radioactivity concentration of truncation portion. Our results suggest that the increase or decrease of % uptake in the truncation data depends on the reconstruction method.

Although zooming acquisition is useful for improving spatial resolution of children and patients with a small heart [2], the acquisition may truncate a patient's body contour. Image reconstructed by truncated projection data on myocardial perfusion SPECT has been considered to be inaccurate. It has been well documented that truncation of the heart in projection data produces artifacts in the reconstructed myocardial image [17, 18]. However, if there is no truncation of the heart, to date, it is unclear how much truncation (area and radioactivity) would affect myocardial image. Based on the results of this study, it suggests that if the area of truncation is < 17.5% and the count of the truncation portion (including bowels and liver) is lower than the myocardial count, if using FBP, the myocardial image is not affected by the truncation artifact.

4.1 Limitations

This study has several limitations. We used only a 180° orbit acquisition. Corrections such as scatter, attenuation, and collimator aperture were not used. There is a possibility that the result may be different by a 360° orbit. The present experimental results were obtained using cylindrical and anthropomorphic torso phantoms. Further clinical studies on patients are needed to confirm the validity of our results in clinical practice, particularly for children, and patients with a small heart.

5. CONCLUSION

We investigated the effect of truncated projection data on the myocardial image in myocardial perfusion SPECT using cylindrical and anthropomorphic torso phantoms for FBP and OSEM. The findings indicated that a prerequisite for truncation data and image reconstruction methods would not affect the myocardial image, when the area of truncation was < 17.5% and the count of the truncation portion was lower than that in the myocardium using FBP. The authors declare no conflicts of interest.

6. FIGURE LEGENDS

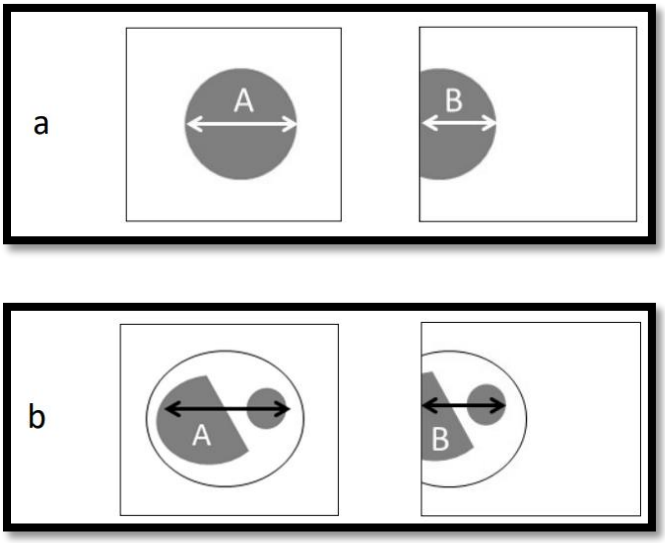

Fig.1 Phantom diameter of the reference image (A) and the truncation image (B) in the FOV.

a. Cylindrical phantom. b. Anthropomorphic torso phantom.

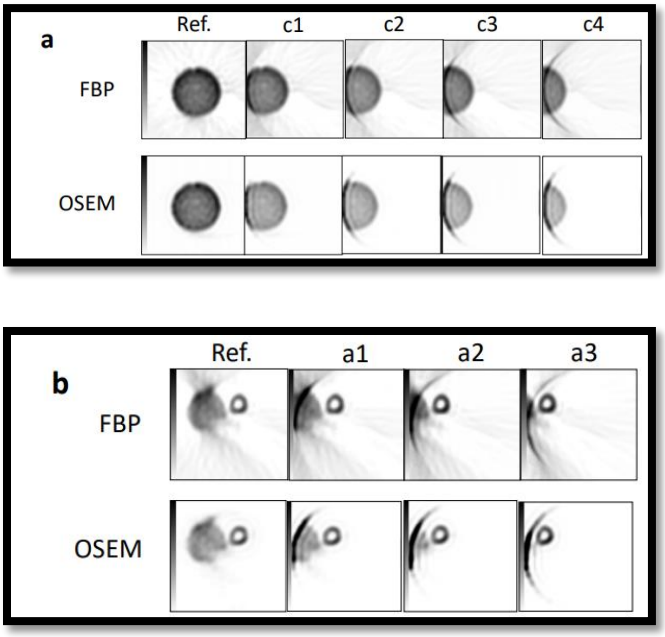

Fig.2 Transverse images of the cylindrical phantom (a) and anthropomorphic torso phantom (b) of the HL radioactivity ratio 1:0:5

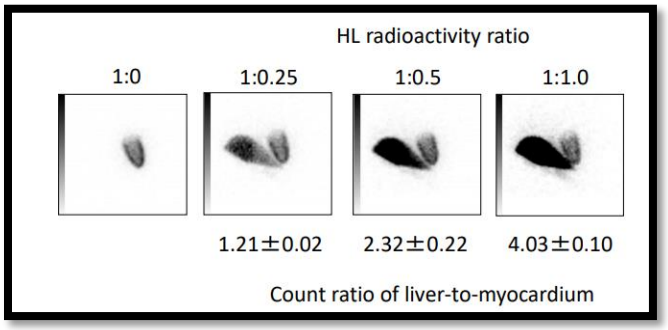

Fig.3 Projection data for the anterior view of the anthropomorphic torso phantom.

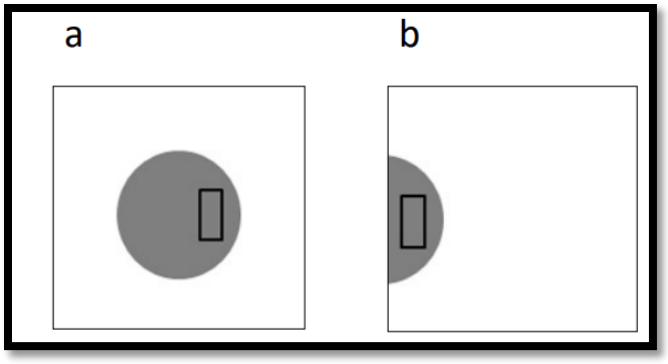

Fig.4 Rectangular region of interest on the cylindrical phantom for uniformity

a. Reference image. b. Truncation image.

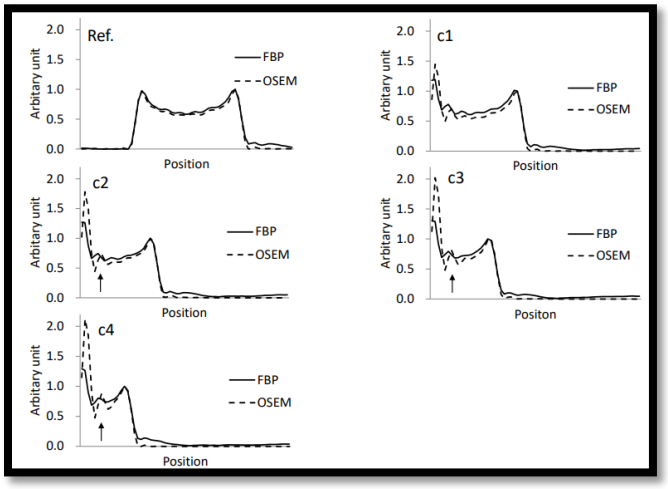

Fig.5 Count profile curves of the cylindrical phantom. The count profile curves were normalized to the maximum count of the phantom edge on the opposite side of the truncation. Larger fluctuation was observed in truncation data of OSEM (arrows).

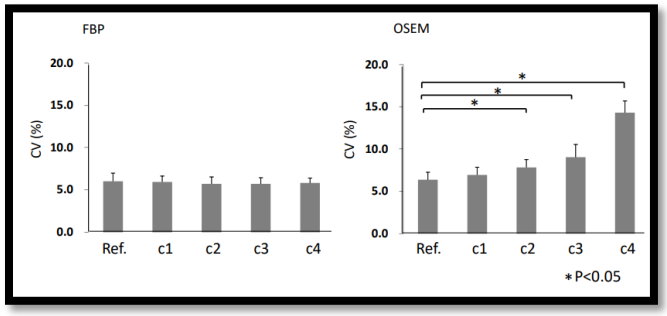

Fig.6 The CVs of the cylindrical phantom

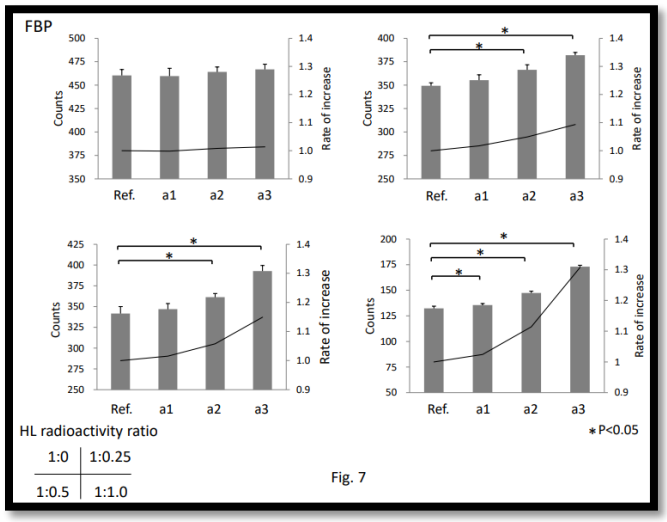

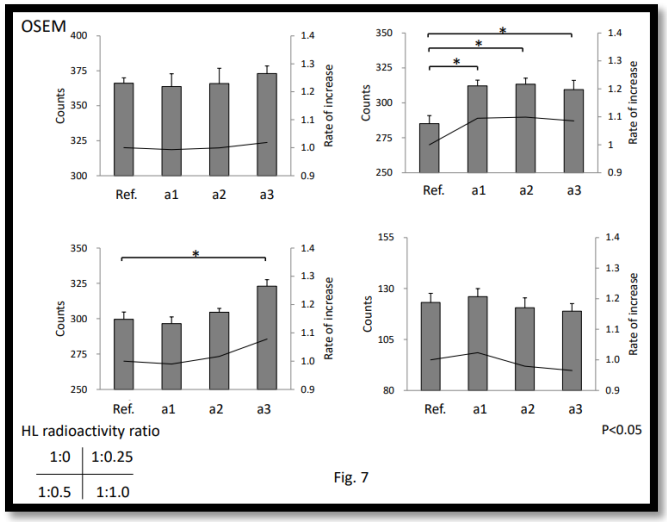

Fig 7. Results of the myocardial count. In FBP, the myocardial counts tended to increase with a larger area and a higher radioactivity concentration of the truncation portion. In OSEM, this tendency was not observed.

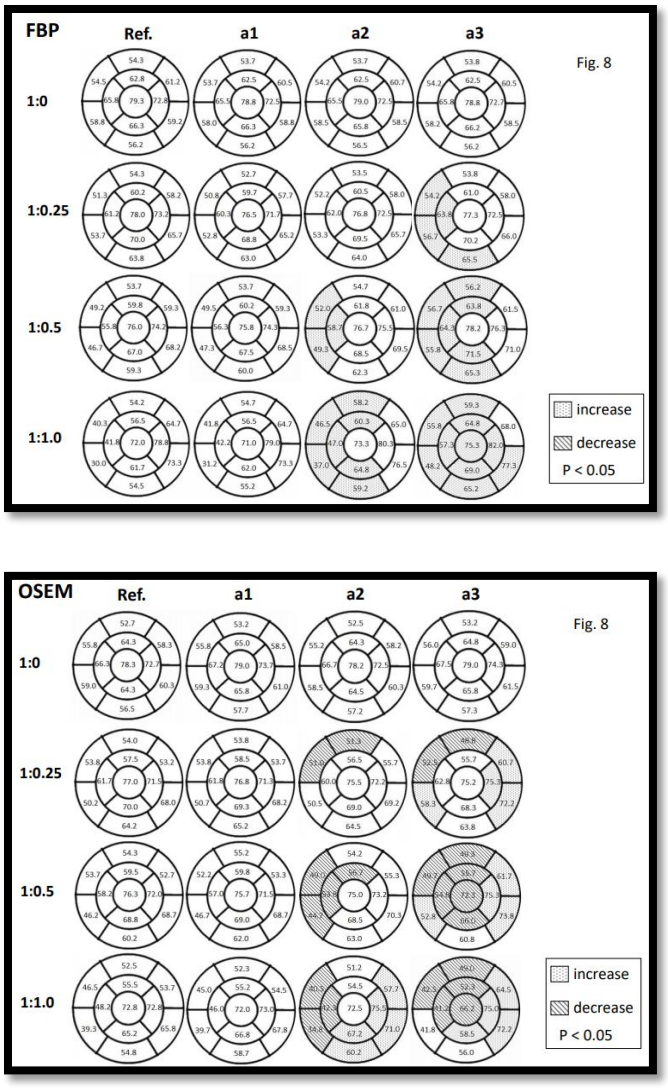

Fig.8 The % uptake of polar map. Dotted and hatched areas are assigned to increase and decrease segment of truncated data compared with reference data.

7. REFERENCES

1. Nishimura T, Nakajima K, Kusuoka H, Yamashina A, Nishimura S. (2008) Prognostic study of risk stratification among Japanese patients with ischemic heart disease using gated myocardial perfusion SPECT: J-ACCESSstudy. Eur J Nuc Mol imaging (35):319-328. https://link.springer.com/article/10.1007/s00259-007-0608-x

2. Nakajima K, Taki J, Higuchi T, Kawano M, Taniguchi M, et al. (2000) Gated SPET quantification of small hearts: mathematical simulation and clinical application. Eur J Nucl Med(27):1372-1379. https://link.springer.com/article/10.1007%2Fs002590000299

3. Gullberg GT, Zeng GL, Datz FL, Christian PE, Tung CH, et al. (1992) Review of convergent beam tomography in single photon emission computed tomography. Phys Med Biol (37):507-534. https://iopscience.iop.org/article/10.1088/0031-9155/37/3/002

4. Manglos SH. (1992) Truncation artifact suppression in cone-beam radionuclide transmission CT using maximum likelihood techniques: evaluation with human subjects. Phys Med Biol (37):549-62. https://iopscience.iop.org/article/10.1088/0031-9155/37/3/004

5. Gregoriou GK, Tsui BM, Gullberg GT. (1998) Effect of truncated projections on defect detection in attenuation-compensated fanbeam cardiac SPECT. J Nuc Med (39): 166-175. http://jnm.snmjournals.org/content/39/1/166.long

6. Celler A, Dixon KL, Chang Z, Blinder S, Powe J, Het al. (2005) Problems created in attenuation-corrected SPECT images artifacts in attenuation maps: A simulation study. J Nucl Med (46):335-344. http://jnm.snmjournals.org/content/46/2/335.long

7. Chen J, Galt JR, Case JA, Ye J, Cullom SJ, et al. (2005) Transmission scan truncation with small-field-of-view dedicated cardiac SPECT systems: Impact and automated quality control. J Nucl Cardiol (5):567-573. https://link.springer.com/article/10.1016%2Fj.nuclcard.2005.04.013

8. Rohmer D, Eisner RL, Gullberg GT. (2006) The effect of truncation on very small cardiac SPECT camera systems. Lawrence Berkeley National Laboratory. http://escholarship.org/uc/item/6cj158t7.

9. Lalush DS, Tsui BM. (2000) Performance of ordered-subset reconstruction algorithms under condition of extreme attenuation and truncation in myocardial SPECT. J Nucl Med (41):737-44. http://jnm.snmjournals.org/content/41/4/737.long

10. Sabondjian E, Stodilka RZ, Belhocine T, King ME, Wisenberg G, et al. (2009) Small field-of-view cardiac SPECT can be implemented on hybrid SPECT/CT platforms where data acquisition and reconstruction are guided b CT.Nucl Med Commun (30):718-726.

https://journals.lww.com/nuclearmedicinecomm/Abstract/2009/09000/Small_field_of_view_cardiac_SPECT_can_be.11.aspx

11. American Heart Association Writing Group on Myocardial Segmentation and Registration for Cardiac Imaging:, Cerqueira MD, Weissman NJ, Dilsizian V, Jacobs AK, Kaul S, et al. (2002) Standardized myocardial segmentation and nomenclature for tomographic imaging of the heart. A

statement for healthcare professionals from the Cardiac Imaging Committee of the Council on Clinical Cardiology of the American Heart Association. Circulation (105):539-542.
https://www.ahajournals.org/doi/10.1161/hc0402.102975?url_ver=Z39.88-2003&rfr_id=ori%3Arid%3Acrossref.org&rfr_dat=cr_pub++0pubmed&

12. Kanda Y. (2013) Investigation of the freely available easy-to-use software 'EZR' for medical statistics. Bone Marrow Transplant(48):452-458.
https://www.ncbi.nlm.nih.gov/pmc/articles/PMC3590441/

13.Maniawski PJ, Morgan HT, Wackers FJ. (1991) Orbit-related variation in spatial resolution as a source of artefactual defects in thallium-201 SPECT. J Nucl Med (32):871-5. http://jnm.snmjournals.org/content/32/5/871.long

14. Liu YH, Lam PT, Sinusas AJ, Wackers FJ. (2002) Differential effect of 180°and 360°acquisition orbits on the accuracy of SPECT imaging: quantitative evaluation in phantoms. J Nucl Med(43):1115-1124.
http://jnm.snmjournals.org/content/43/8/1115.long

15. Taki J, Fujino S, Nakajima K, Matsunari I, Okazaki H, et al. (2001) 99mTc-sestamibi retention characteristics during pharmacologic hyperemia in human myocardium: comparison with coronary flow reserve measured by Doppler flowire. J Nucl Med (42):1457-1463. http://jnm.snmjournals.org/content/42/10/1457.long

16. Storto G, Soricelli A, Pellegrino T, Petretta M,Cuocolo A. (2009) Assessment of the arterial input function for estimation of coronary flow reserve by single photon emission computed tomography: comparison of two different approaches. Eur J Nucl Med (36):2034-2041. Assessment of the arterial input function for estimation of coronary flow reserve

17. Wosnitzer B, Gadiraju R, Depuey G. (2011) The truncation artifact. J Nucl Cardiol (18):187-191. https://link.springer.com/article/10.1007%2Fs12350-010-9290-7

18. Tsougos I, Alexiou S, theodorou K, Valotassiou V, Georgoulias P. (2015) The prevalence of a false-positive myocardial perfusion stress SPET test in a skinny patient, induced by projection truncation. Hell J Nucl Med (18):79-80. https://pubmed.ncbi.nlm.nih.gov/25679080/e.

Article Citation:

Authors Name. Masahisa Onoguchi. Prerequisite for projection data and reconstruction not to cause truncation artifacts in myocardial perfusion single- photon emission computed tomography: Phantom study. SJC 2020;1(3): 82 - 89
DOI: doi.org/10.46978/sjc.20.1.2.14